Electron Photodetachment Spectroscopy of Trapped Negative Ions

DONNA M. WETZEL and JOHN I. BRAUMAN*

Chemistry Department, Stanford University, Stanford, California 94305

Received October 14, 1986 (Revised Manuscript Received March 2, 1987)

Contents

Donna M. Wetzel obtained a B.S. in chemistry from Purdue University, Indianapolis. Her undergraduate research involved carbanion chemistry, metal ammonia reduction of aromatic compounds, and the conformational analysis of unsaturated ring systems using NMR techniques. Currently she is a doctoral student in the chemistry department at Stanford University. Her thesis work involves study of the spectroscopy and thermochemistry of gas-phase negative ions using ICR and photodetachment spectrometry.

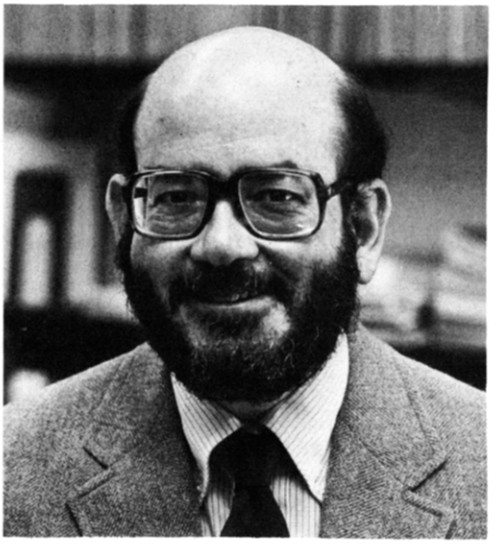

John I. Brauman received his undergraduate degree from MIT (1959) and his Ph.D. from the University of California at Berkeley (1963). Following a postdoctoral appointment at UCLA he joined the faculty at Stanford University where he is currently J. G. Jackson–C. J. Wood Professor of Chemistry. His research interests are in the areas of mechanistic chemistry and spectroscopy, especially for ionic reactions in the gas phase.

I. Introduction

Negative ions provide a fertile field for spectroscopic investigation; relatively little is known about their structure, electronic states, or absolute energetics. Electron photodetachment is a powerful method for exploring all of these areas. In this paper we cover one restricted aspect of the field: electron photodetachment using trapped ions.

When negative ions are irradiated, the following process can occur:[1]

$$A^- + h\nu \rightarrow A + e^- \qquad (1)$$

Two general types of experiments can be used to monitor this process. In photodetachment spectroscopy, the process in eq 1 is monitored as a function of photon energy. In photoelectron spectroscopy, a fixed-frequency photon is used to induce the electron detachment and the energy of the photoelectron is measured. Each technique provides useful and sometimes complementary information.

This paper focuses on the experimental technique of photodetachment threshold spectroscopy of molecular ions formed and irradiated in an ion trap. Those results more recent than (or not discussed in) the last review of this topic[2a] are featured. We have not included a comprehensive discussion of recent experiments involving both photodetachment threshold spectroscopy and photoelectron spectroscopy of ion beams. Rather, results of a select few of these types of experiments are mentioned in conjunction with related ion-trap experiments. Interested readers should consult the most recent review of photodetachment experiments involving negative ion beams[2b] and representative recent

0009-2665/87/0787-0607$06.50/0

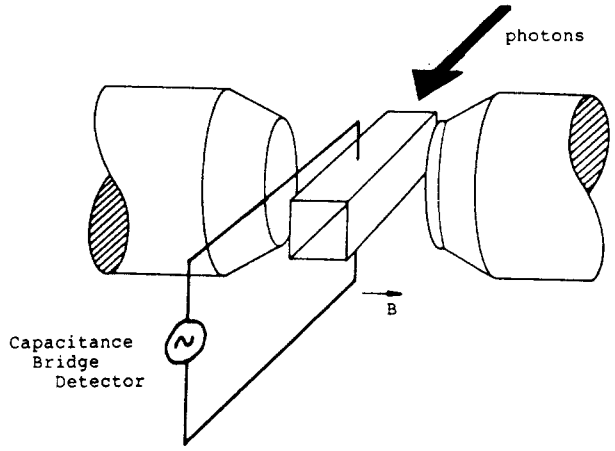

Figure 1. Schematic of ICR spectrometer. The plates of the cell are electrically isolated from each other.

papers by workers in this field.[137] Reviews by Miller[3] (which discusses both photodetachment and photodissociation of ions) and Berry and Leach[4] (which treats electron attachment and detachment processes) provide detailed descriptions of photodetachment as well.

Photodetachment spectroscopy is a well-established optical technique[5] for the measurement of electron affinities.[2,6] Recently, chemical methods involving charge-transfer equilibrium measurements[7] (using high-pressure mass spectrometry (HPMS)) have been used to determine the electron affinities for a large number of molecular anions. The contribution from Kebarle in this issue discusses the use of chemical methods to determine electron affinities.

The first section of this paper presents those aspects involved in ion formation and irradiation and in the measurement of a photodetachment spectrum. Threshold laws and cross-section calculations, derived from models of the optical electron detachment process, are then considered. The experimental results covered in this paper fall into three broad categories: those experiments which involve transitions to electronic excited states of anions or neutrals, those experiments in which the photodetachment onset measured an electron affinity and resulted in thermochemical information, and finally those experiments which probe an electron detachment process fundamentally distinct from optical photodetachment, namely, vibration-induced electron detachment.

II. Experimental Considerations

A. Principles of ICR

Ion cyclotron resonance (ICR) spectrometry[8] has been the predominant experimental method used to study the photodetachment spectroscopy of trapped negative ions.[9] The apparatus, a simplified schematic of which is shown in Figure 1, consists of a cell, encased in a high-vacuum can, positioned between the pole faces of an electromagnet. Although the ions travel at thermal velocities ($\sim 10^4$ cm s^{-1}), the magnetic field constrains ion motion to circular orbits (with a frequency proportional to the ions's charge-to-mass ratio and the magnetic field strength). This constrained motion and the presence of electric fields resulting from the potentials applied to the cell plates serve to trap the ions for periods of seconds. Ions can be formed by a wide variety of procedures: electron capture or dissociative electron capture by neutrals or by ion–molecule reactions of these primary ions. The abundance of reactions available for forming ions makes ICR spectrometry well suited for the study of polyatomic anions and closed-shell anions. Because ions are formed via chemical reactions, however, the experiment samples a broad, often Boltzmann, internal energy distribution rather than a well-defined single state population. Typical neutral gas pressures employed are 10^{-8}–10^{-5} Torr.

Ions are detected by incorporating the upper and lower plates of the cell into a capacitance bridge circuit.[10] The basis of the detection scheme is the coherent cyclotron motion of all ions of a given charge-to-mass ratio. When the ions are brought into resonance with a driving radio frequency detection oscillator,[11] the cyclotron orbits align in phase, thus inducing an image current on the lower plate. This image current is converted to a voltage and measured by use of phase-sensitive detection. The detection scheme avoids mass discrimination and does not rely on any particle collection. The response of the capacitance bridge detector (CBD) to the number of ions in the analyzer region of the cell has been shown to be linear.[12] A problem encountered in the use of the CBD for measuring changes in ion concentration is that the exact resonance frequency is very sensitive to the number of ions in the cell, and the CBD signal has a very narrow bandwidth. Thus, photochemically induced ion loss is often accompanied by a frequency shift, and small resonance frequency shifts can result in a large signal change because the detection frequency no longer corresponds to the signal maximum. This problem has been overcome by use of a frequency lock system,[13] a negative feedback circuit involving magnetic field modulation, which provides a continuous correction signal to the frequency generator to ensure the detection frequency always corresponds to the exact resonance frequency.

The CBD can be operated in either continuous or pulsed mode. The major difference between these modes of operation is temporal control. In continuous mode operation, primary ions are continuously generated from an electron source. Since primary ions are continuously formed, all secondary ions are also continuously formed. The rates of ion formation and nonreactive ion loss (e.g., colliding with the cell plates) establish a steady-state ion concentration. This ion population is continuously detected during the experiment. Any process in addition to nonreactive loss, for instance, photodetachment resulting from interaction with photons, alters this steady-state ion concentration. In pulsed-mode operation, the experiment is temporally controlled by a series of pulses. Primary ions are formed for a specified period of time by a pulse of electrons. This collection of ions can then react with neutrals to form secondary ions, interact with photons, or be lost to the walls of the cell. At some later time ions are detected by a short resonance frequency detection pulse. The temporal decay, by whichever process, can be measured in a pulsed experiment because primary ions are formed only once. Typical time resolution is milliseconds.

The advantage of continuous-mode operation is the signal-to-noise ratio, inherently better than in pulsed-mode operation because of constant detection. How-

ever, because one has temporal control over the events in the ICR cell, pulsed-mode operation is advantageous in certain experiments. For example, in a system in which the primary ion has a photodetachment threshold lower in energy than the secondary ion, double-resonance techniques[14] selectively remove the primary ions, after the secondary ions are formed but prior to irradiation, so that the detected ion signal is solely a function of the secondary ion's photochemistry. In pulsed-mode operation it is also possible to measure absolute rather than relative cross sections (see below). It is likely that Fourier transform[15] (FT-ICR) will play an increasingly important role in pulsed experiments since all the ions can be monitored at once.

B. Photodetachment Experiments

Optical electron detachment experiments can be conducted by using either mode of operation. In general, continuous mode operation is used to measure photodetachment cross sections, since small ion signal changes (0.5%) can be reliably measured. In the experiment, the photons enter the ICR cell (see Figure 1) through a window at the end of the high-vacuum can. This arrangement results in large spatial overlap and, with long trapping times, allows measurable ion decreases with readily available photon fluxes.

The "raw data" in an optical photodetachment experiment are the ion signals with and without irradiation. In order to convert these data into a photodetachment spectrum, the observed fractional signal decrease must be related to the photodetachment cross section. The probability of photodetaching an electron from a negative ion is[16]

$$P(\lambda) = 1 - N/N_0 = 1 - \exp(-k_p t) \qquad (2)$$

where N is the ion signal with irradiation, N_0 is the ion signal without irradiation, t is the time an ion spends in the photon beam, and k_p is the rate constant for photodetachment given by[17]

$$k_p(\lambda) = g\ \sigma(\lambda)\ \rho(\lambda) \qquad (3)$$

In this equation, g is the geometric overlap factor for overlap between the ion cloud and the photon beam, $\sigma(\lambda)$ is the cross section for photodetachment, and $\rho(\lambda)$ is the photon flux. Substituting eq 3 into eq 2, rearranging, and taking logarithms yield an expression for the cross section in terms of the quantities measured during a photodetachment experiment:

$$\sigma(\lambda) = (t/g)\ \ln\ (N_0/N)/\rho(\lambda) \qquad (4)$$

Photodetachment spectra consist of the wavelength dependence of this cross section.

Since in the continuous-mode experiment t, the time an ion spends in the photon beam, is not accurately known, only relative cross sections can be determined. In contrast, in a pulsed-mode experiment the irradiation time can be controlled and t is accurately known. One needs to measure the absolute value of the photon flux and to determine g, the geometric overlap factor, in order to measure an absolute cross section. This has been accomplished by the measurement[18] of ion signals in a photodetachment experiment involving HS^-. The absolute photodetachment cross section for this ion has been measured in a beam experiment.[19] The value of g was determined by using this absolute cross section as a calibration for the ICR experiment.

The internal energy content of the ions in an ICR is not always well-defined. This issue is of particular concern when exothermic reactions are involved in ion formation. Until recently it was generally assumed that for ion–neutral collisions (which are in the Langevin–ADO limit[20]) a few collisions were adequate to relax completely an excited ion. However, the results of an IR photodissociation experiment involving CH_3OHF^- suggested that ~100 collisions between the ion and bath gas (methyl formate) were required to remove excess internal energy.[21] Recent, quantitative ICR experiments designed to measure quenching rate constants[22] gave further evidence that polyatomic systems can have (surprisingly) low collisional efficiencies.[23] These results indicate that internal energy may not always be relaxed during the time ions are trapped in the ICR cell, and this should be taken into account in experiments designed to measure equilibrium[24] and threshold quantities. Nevertheless, photodetachment threshold assignments are usually reliable, since the transitions resulting from internally excited ions generally do not obscure the predominant 0–0 onset.

The preceding paragraphs described an optical photodetachment experiment. As discussed later, electron detachment from anions can also be induced by infrared activation. This process is fundamentally different from optical photodetachment. Experiments measuring this phenomenon can also be conducted by using ICR spectrometry. When high-powered, pulsed lasers are used, ICR must be operated in the pulsed mode. The laser can be triggered by the same timing circuitry used to generate and detect ions. As in an optical photodetachment experiment, the ion signal at the resonance frequency is measured in the presence and absence of irradiation. Indirect evidence for electron detachment is provided by a decrease in the particular ion signal without the observation of any photoproducts. Direct evidence is obtained by chemical trapping methods: carbon tetrachloride readily captures free electrons to form chloride ion. Electron detachment is then detected as an increase in the chloride ion signal following infrared irradiation.[25] Time scans conducted with and without irradiation yield information on whether secondary photochemistry or parent ion regeneration occurs during or after the irradiation period.

A new experimental technique that involves trapping and optically exciting ions in a radio frequency octupole trap has allowed measurement of radiative (both electronic and vibrational) lifetimes for negative ions.[26,27] In experiments of this type, the radiative decay is measured indirectly by probing the excited-state population; laser photodetachment serves as the probe. The selection of photon energies at values below the ground-state threshold ensures that only ions in excited states will detach an electron. Thus the excited-ion population can be inferred from the magnitude of the photodetachment signal. Radiative lifetimes of excited CH_2^- and CH^- have been measured by using this technique.[26,27]

Optical electron detachment experiments yield thermochemical and spectroscopic data. The results from these types of experiments are discussed in sections IV and V. Infrared photon-induced electron de-

tachment is a relatively new phenomenon and is discussed separately in section VI.

III. Models for Optical Photodetachment

A. Threshold Laws

Optical detachment of an electron is a bound-free transition from an anion to the corresponding neutral and free electron. The photodetachment spectrum is integral (the observed detachment at a given wavelength is the sum of all vibronic and electronic transitions which occur at that energy) and, in general, monotonically increases with energy above threshold. Near threshold, the cross section at each wavelength corresponds to the sum of all allowed transitions. In order to assign the experimentally observed onset to the threshold of a photodetachment transition, it is useful to make comparisons with modeled or calculated cross sections. This approach is especially useful when the experiment involves a large instrumental bandwidth. In such cases, the threshold value that results in a best fit of the calculated cross section to the experimental data is taken as the threshold energy for the transition.

Wigner[28] solved the functional dependence of collision cross section near threshold for a process yielding two final particles and showed that it depends only on the long-range forces between the products. In photodetachment from anions, the departing electron experiences a long-range potential due to polarization with the neutral (which falls as r^{-4}, neglecting charge–dipole interactions) and the centrifugal potential of the "collision complex". It is this centrifugal potential, proportional to $l(l + 1)/r^2$, that dominates the long-range forces. The resulting form of the cross section near threshold for this case is

$$\sigma(E) \propto k^{(2l+1)} \tag{5}$$

where k is the magnitude of the linear momentum of the photoelectron. Since $k = (2m\Delta E)^{1/2}/\hbar$, where ΔE is the energy above threshold

$$\sigma(E) \propto (\Delta E)^{l+(1/2)} \tag{6}$$

This functional form can be applied to atomic anions with l, representing the quanta of angular momentum in the photoelectron, determined by the conventional dipole selection rules to be ±1 of the angular momentum quantum number of the orbital from which it was ejected. This yields a threshold law that predicts the shape but not the magnitude of the cross section as a function of energy above threshold. Other treatments have also been applied to the case of atomic photodetachment.[29]

Geltman[30] derived a threshold law for diatomic negative ions having an equivalent functional form to that shown in eq 5. Reed et al.[31] used group theory to extend Wigner's threshold law to polyatomic anions. The atomic orbital angular momentum quantum number is replaced by an "effective angular momentum" quantum number of the highest occupied molecular orbital (HOMO) from which the electron is detached, determined by a group theoretical approach. The irreducible representation of the HOMO under the point group of the anion defines the effective angular momentum, l'. For example, the totally symmetric irreducible representation has $l' = 0$, and orbitals whose irreducible representation is labeled as x, y, or z have $l' = 1$, etc. Again, when dipole selection rules are used to connect the angular momentum of the departing photoelectron to the HOMO from which it was ejected, $l^* = l' \pm 1$ and

$$\sigma(E) \propto (\Delta E)^{l^*+(1/2)} \tag{7}$$

This law does not predict the relative intensities of competing allowed transitions. In those cases where more than one l^* is possible, for instance, when the HOMO contains contributions from different irreducible representations, the resulting functional form that rises more rapidly with increasing energy will usually dominate the cross-section behavior, assuming the contribution to it is reasonably substantial.[32] A photoelectron resulting from an s (or s-like, totally symmetric) orbital exhibits p wave behavior; $l' = 0$, $l^* = 1$, and the cross section rises as $\Delta E^{3/2}$. Again, this threshold law predicts only the shape of the cross section. Neither this nor the Wigner law describes the cross-section behavior much above threshold. For molecular anions of low symmetry the law has limited application.

Experiments involving polar molecules show cross-section behavior different from that predicted by the Wigner law.[33] Engelking[34] has proposed that this anomalous behavior is due to a significant contribution to the long-range potential from a charge–dipole interaction, ignored in the Wigner treatment. Strong coupling occurs when the departing electron leaves behind a molecule having an orientable dipole moment and parity degeneracy (symmetric top rotors possessing internal angular momentum K along the dipole axis satisfy this condition, as do diatomics with an electronic angular momentum along the molecular axis). Engelking's model describes this coupling as an r^{-2} attractive dipole potential and results in a modified threshold law. The interaction involves a coupling of the electron's angular momentum, l, to individual molecular levels with quantum numbers J and K, respectively, for overall rotations and rotations about the axis containing the molecular dipole. The model predicts a threshold law $\sigma \sim k^x$, where $x < 1$, dependent on the molecular dipoles and rotational threshold considered. Computations compare well to experimental measurements[35] of OH^-, although only in a limited energy range above threshold. This theory is not an attempt to describe overall cross-section behavior but is restricted to low kinetic energies in the vicinity of a rotational threshold. An extension to the theory[36] includes the effects of rotational doubling. Rotational doubling (spin, orbital, or molecular) quenches the electron–dipole interaction. One might predict a "partial recovery" to the Wigner threshold behavior by including these effects. The calculations show that doubling (in the OH^- system) breaks the modified threshold law, but not necessarily to that predicted by the Wigner law.

B. Cross-Section Calculations

Reed[31] extended the threshold law formalism to present the first calculation of the cross section for photodetachment for molecular negative ions. The photodetachment process is treated as a one-electron, dipole-allowed transition; the cross section is obtained from the calculated matrix element

$$\langle \psi_i | r | \psi_f \rangle \quad (8)$$

where ψ_i is the initial state, r is the dipole operator, and ψ_f is the final state consisting of the neutral molecule plus free electron. The free electron is treated as a plane wave and orthogonalized to the HOMO of the anion. Input parameters for the cross-section calculation include the atomic orbital coefficients in the HOMO, orbital exponents for each atom in the anion,[37] and the photodetachment threshold energy (when the value of the threshold energy is varied to obtain a fit with experimental data, photodetachment onsets can be assigned). The calculated photodetachment cross sections agreed well[31] with measured OH^-, O_2^-, and $C_5H_5^-$ data.

Woo developed a model,[38] the zero-core-contribution (ZCC) model, to calculate the absolute photodetachment cross section of atomic negative ions. He has extended this model to calculate cross sections for homonuclear diatomic negative ions,[39] heteronuclear diatomics,[40] and the effects of fine structure levels and higher electronic states of the anions and neutrals in atomic systems.[41] The ZCC model is also a one-electron model, depicting a negative ion as a neutral and an "extra" electron. The wave function of this extra electron outside a radius r_0 (where r_0 defines the core and is chosen as proportional to the root-mean-square radius of the outermost occupied orbital of the neutral atom, or, for the case of a diatomic, the region of two overlapping atoms) is obtained by solving a constant potential Hamiltonian; inside the core it is assumed to be zero. For atomic systems the model requires only three input values: r_0, E, the threshold energy for each photodetachment channel, and l, the angular momentum quantum number of the outermost "detachment orbital". For diatomic systems, in addition to knowledge of the molecular orbital of the extra electron, one must know the vertical detachment energies corresponding to each vibrational transition contributing to the total cross section, the size of the neutral atoms, and an equilibrium internuclear potential for the ion and neutral (a Morse potential is typically assumed). The ZCC model calculates the energy dependence of the total cross section, partial cross sections for each channel opening, and the angular distributions of each channel. The model yields good agreement (within the estimated errors of the theories and experiments) in comparison with experimental data of 20 atomic anions (from the IIIA–IVA (3 and 4) families, all having p outermost occupied orbitals) as well as with calculations by Rau and Fano[42] and Hotop.[43] On diatomic systems, calculated cross sections agree with the experimental data of OH^- to within 30%, with that of SH^- within 20%, and to the data of O_2^- within a factor of 2. Further extension of the model to triatomic systems of the form XYX is under way.

IV. Thermochemical Information Obtained through Photodetachment

A. Electron Affinities and Related Thermochemical Parameters

Electron photodetachment spectroscopy can be used to determine an important thermochemical parameter, the electron affinity of the neutral photoproduct. Molecular electron affinities are one of the critical links between ion thermochemistry and neutral thermochemistry. Knowledge of this thermochemistry plays a major role in understanding the kinetics and mechanisms of ion–molecule reactions, allowing one to predict the position of equilibria, likely reaction intermediates, reaction rates, and stabilities of reactive intermediates (radicals). In addition, molecular electron affinities indicate the relative stabilities of the corresponding anions for chemically related species. Recent experiments make use of the electron affinities measured by photodetachment to infer structural information and derive solvation energetics for solvated anions.[18,67,68,79,82]

The electron affinity is the minimum energy required to remove an electron from the anion in its ground rotational, vibrational, and electronic state to form the neutral in its ground rotational, vibrational, and electronic state and an electron with zero kinetic and potential energy. The most intense onset observed in a photodetachment spectrum corresponds to the threshold for the vertical transition between the anion and the neutral.[44] If there is a substantial geometry change in going from the negative ion to the neutral, the 0–0 transition, which corresponds to the adiabatic electron affinity, will not be the most intense onset in the photodetachment spectrum and may even be too weak to be observed. If there is substantial population in higher vibrational states that have strong transition probabilities, an onset at photon energies less than the adiabatic transition may appear in the spectrum. In those cases where the experimental onset cannot be definitively assigned as the 0–0 transition, the electron affinity is reported as either an upper or lower bound to the adiabatic electron affinity.

The growing number of experimentally determined molecular electron affinities[2,7] and proton affinities of negative ions[45] makes the derivation of neutral homolytic bond dissociation energies via thermochemical cycles a particularly attractive and comprehensive technique. This cycle[46] connects the electron affinity of the radical and the proton affinity of the corresponding anion to the homolytic bond dissociation energy ($D°$):

$$D°(\text{A–H}) = \text{EA}(\text{A}^\bullet) + \text{PA}(\text{A}^-) - \text{IP}(\text{H}^\bullet) \quad (9)$$

Thermokinetic methods[47] (involving abstraction or pyrolysis reactions) are primary methods used to determine bond energies; these are generally in good agreement with the $D°$'s determined by thermochemical cycles. Some discrepancies do exist, and recently attention has been directed to the systematic discrepancies in the set of RO–H bond energies in alcohols.[48a] The $D°$'s determined for this series of compounds via thermochemical cycles were uniformly 2 kcal/mol lower than those determined by thermokinetic techniques. Results from IR branching ratio experiments[48b] and kinetic rate measurements[48a] indicated that the gas-phase acidity of HF (used to anchor the relative gas-phase acidity scale and thus convert relative to absolute proton affinities) was inaccurately assigned and was the source of the anomalous bond energy values. The $D°$ of methanol determined thermochemically was assumed, instead, to be correct,[49] leading to revised values for the alcohol acidities. The experimentally determined electron affinities appeared not to be a source of error.

TABLE I. Thermochemical Parameters[a] of Substituted Benzene Compounds (kcal/mol)

A	$D°$(A–H)	EA(A•)	PA(A^-)
C_6H_5NH	92.8 ± 2.6	39.3 ± 0.7	367 ± 2[b]
C_6H_5N	92.1 ± 2.3	33.7 ± 0.3	372 ± 2[c]
$C_6H_5CH_2$	87.3 ± 2.3	19.9 ± 0.3	381 ± 2[b,d]

[a] Unless otherwise stated, values obtained from ref 57. [b] Reference 58. [c] Reference 59. [d] Reference 48.

B. Applications to Chemical Species

Literature values for the N–H bond dissociation energy in HN_3 and the enthalpy of formation of the azide radical are still in dispute. The $\Delta H_f°(N_3^-)$ had been estimated,[50] from a Born–Haber cycle, as 34.8 ± 1 kcal/mol and, by dissociative electron attachment[51] to HN_3, as ≤46 ± 7 kcal/mol. A direct measurement of the proton affinity of the azide anion and the electron affinity of the azide radical would result in reliable thermochemical data. To this end, the electron affinity of the azide radical was measured by photodetachment spectroscopy.[52] The resultant[52] EA, 62.1 ± 2.8 kcal/mol, led to thermochemical values much higher than previous literature values. That photodetachment measurement, however, was made difficult due to other anions present during the experiments. Recent dissociative electron attachment experiments indicated that benzyl azide is an efficient and clean source of azide anion.[53] Azide anion generated in this way enabled unambiguous assignment of the EA, 63.7 ± 1 kcal/mol, from the photodetachment spectrum.[53] Agreement with the previous EA value indicated that proper accounting of the contributions to the photodetachment spectrum had been taken. This EA, in combination with the proton affinity of the azide anion[54] yields a $D°(N_3–H)$ of 92.2 ± 4.6 kcal/mol. The $\Delta H_f°(N_3^-)$, obtained from the proton affinity,[54] was 48 ± 2 kcal/mol. While these values are considerably higher than the previous values, they are arguably more reliable since they are direct measurements and are more consistent with the thermochemical values of related specis (the $D°(H_2N–H)$ for ammonia[55] is 107 kcal/mol; the $D°$(HN–H) for amide[56] is 95 kcal/mol).

Recent photodetachment studies on the anilide, benzyl, and phenylnitrate anions[57] resulted in the derivation of the N–H and C–H bond dissocation energies for toluene, aniline, the anilide anion, and the anilide radical. These, along with the measured EAs and proton affinities[58,59] are displayed in Table I. The $D°$'s of aniline and the anilide radical are an interesting pair. The N–H $D°$ of anilide radical may be thought of as the "second" N–H bond strength in aniline. As shown in Table I, the energy required to break the first N–H bond in aniline is remarkably similar to that of the second N–H bond. The thermochemistry of ammonia is very different; the second N–H $D°$ is approximately 12 kcal/mol less than[55,56] the first N–H. The difference between these systems is due mainly to resonance stabilization. Stabilization of the anilide radical effectively lowers the first bond dissociation energy relative to the second, thus equalizing the two.

Such resonance stabilization seems to be unimportant for organosilane compounds. Preliminary ICR experiments measuring the proton and electron affinities of silyl and organosilyl anions and radicals, respectively,[60] indicated that the bond energies of alkyl- and aryl-substituted silane compounds are essentially the same, implying that organosilyl radical stabilities are unaffected by substitution. Earlier experiments on alkyl-substituted alcohols[61] and mercaptans[62] also found bond strengths to be independent of alkyl substitutions. The observation that alkyl and aryl substitution affords no special stabilization to organosilyl radicals might be related to the fact that the extra electron lies in a nonbonding orbital.[63] The measured electron affinities of the organosilanes studied gave evidence of a methyl effect which destabilizes silyl anions. Such an effect has been evoked to explain magnetic circular dichroism results involving silyl substituents as π electron donors and acceptors.[64]

Gas-phase acidities and electron photodetachment threshold measurements on family IVA (4) trimethyl hydrides[65] resulted in the first direct determination of the bond dissociation energy of trimethyltin hydride, as well as the bond dissociation energies for trimethylgermane and trimethylsilane hydrides. The EA's of these trimethyl metal hydrides were found to be lower than their tetrahydride analogues, giving further evidence of methyl destabilization in family IVA (4) anions. The electron affinities were found to increase in going down the IVA (4) family, as was the case with the EA's of the bare IVA (4) atoms, recently determined by photoelectron spectroscopy.[66] For these atomic data, the decrease in electron affinity was attributed to a breakdown in L–S angular momentum coupling in going to heavier atoms. This explanation may hold true for the hydrides.

C. Energetics and Structural Information of Complex Ions

Golub and Steiner, in 1968, measured the photodetachment spectrum of a solvated anion, water-solvated hydroxide ion in a crossed-beam experiment.[67] This experiment showed the utility of electron photodetachment as a probe of the energetics of complex ions. However, the data, slowly rising cross sections at threshold (attributed to dissociative photodetachment), are difficult to interpret.

Recently, photodetachment experiments involving solvated anions of the form $[ROHF]^-$ have been undertaken, with the intent to probe both structure and energetics.[18,68] The reactivity of these complex ions[69] indicated that the complexes consist of proton-bound fluoride and alkoxide ions. A series consisting of ions in which R corresponded to the alkyl groups methyl, ethyl, isopropyl, *tert*-butyl, neopentyl, and benzyl were generated and irradiated in an ICR.[68] Only the complex ion with R = benzyl was found to detach.

In order to use the photodetachment results to gain structural information about the $[ROHF]^-$ systems, namely, whether the complex ion resembles alcohol-solvated fluoride ion, ROH---F^-, or HF-solvated alkoxide ion, RO^----HF, one must assume that Franck–Condon factors play an important role in the detachment process.[44] Poor Franck–Condon overlap precludes detachment to products whose geometry differs substantially from that of the anion.

Figure 2 illustrates the scheme used to rationalize the photodetachment results from reference 68. The energies of RO^----HF and ROH---F^- are similar, since the acidities of ROH and HF are similar. The energies of

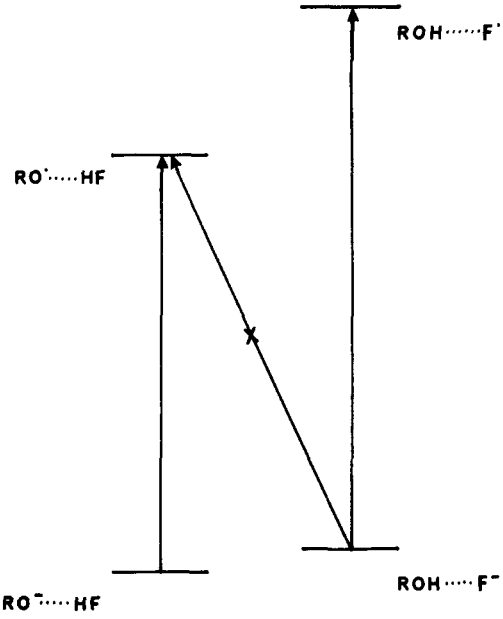

Figure 2. Relative energies and photodetachment transitions for solvated anion and neutral complexes.

the neutral complexes, RO---HF and ROH---F, are very different, however, owing to the very large differences in the H–F and RO–H bond strengths. Thus the vertical photodetachment energies should be very different: the RO^----HF → RO---HF vertical detachment transition should be much lower in energy than the ROH---F^- → ROH---F transition. The vertical detachment threshold for the alcohol-solvated fluoride ion, ROH---F^- → ROH---F, is too high to be observed.[70] Poor Franck–Condon overlap precludes the observation of the adiabatic transition, ROH---F^- → RO---HF, whose threshold energy is accessible in the experiment. The vertical detachment threshold for the HF-solvated alkoxide ion, RO^----HF → RO---HF, is, however, accessible in the experiment. Therefore, those $[ROHF]^-$ ions for which photodetachment can be measured (cross sections having significant intensity) must resemble HF-solvated alkoxide ions. Since photodetachment was observed for the complex ion in which R = benzyl, this anion has the structure of HF-solvated benzyl oxide ($C_6H_5CH_2O^-$---HF). The other systems resemble alcohol-solvated fluoride ions (ROH---F^-). These photodetachment results also reflect the known relative gas-phase acidities[48] of the alcohols and HF in that the bridging proton is more closely bound to the more basic anion in the $[ROHF]^-$ complex.

The photodetachment threshold of the HF-solvated benzyl oxide ion was used to derive the solvation energy of the complex ion. Figure 3 illustrates the thermochemical parameters involved in the determination of the solvation energy of the complex anion. The electron affinity of benzyloxy radical,[68] 49.4 ± 0.3 kcal/mol, the electron affinity of the HF-solvated benzyl oxide ion,[68] 70 ± 2 kcal/mol, and the solvation energy of the neutral complex[71] result in a solvation energy of the benzyl oxide ion of 29 ± 3 kcal/mol. With the use of the enthalpy of proton transfer from HF to benzyl oxide ion[58] and the solvation energy, a fluoride binding energy of 31 kcal/mol was derived, which compares favorably to predictions by Larson and McMahon.[72] Photodetachment of the methanol-solvated methoxide ion resulted in an EA determination[18] of 52 ± 2 kcal/mol.

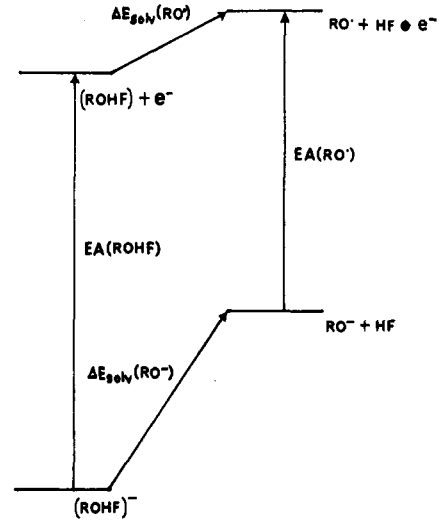

Figure 3. Relationship among electron affinities and solvation energies for solvated anions.

With the use of the thermochemical cycle illustrated by Figure 3, a solvation energy of 19 ± 3 kcal/mol was derived.[18] This compares well to that value reported by Bartmess et al.[73] Very recent HPMS experiments[49] report 28.8 kcal/mol as the solvation energy of the methanol-solvated methoxide.

Poor Franck–Condon overlap between the anion and the neutral has been evoked[74] to explain the absence of a photodetachment onset for the sulfur hexafluoride ion, SF_6^-. No detectable detachment was observed in the ICR experiment[74] using irradiation in the spectral region 300–1100 nm. On this basis as well as kinetic[75] and lifetime evidence[76] a large geometry change and loose structure was proposed for SF_6^-. SCF calculations[77] predict a large difference in the S–F bond lengths for the radical and the anion, and a vertical transition energy much higher than the adiabatic electron affinity. Consistent with previous suggestions,[74] recent studies on charge-transfer reactions involving SF_6^- indicate a large kinetic barrier to electron transfer.[78] The low efficiency reactions make determination of the electron affinity of SF_6 by bracketing techniques difficult. However, HPMS experiments[78] have resulted in a determination, $EA(SF_6)$ = 24.2 ± 2.3 kcal/mol.

Photoelectron spectroscopy has been used to measure the photodetachment spectrum of the NH_4^- ion.[79] It contained only one major peak and thus resembled the spectrum of free hydride ion red-shifted[79] by 8.3 kcal/mol. This red shift corresponds to the solvation energy afforded hydride by the NH_3. Because the detachment transition was presumed to lie near the dissociation limit of NH_4 neutral, the magnitude of the shift represented an upper bound to the solvation energy. This measured value agreed well with calculated solvation energies.[80]

The results are consistent with both calculations[80] and FT-ICR deuterium-labeling experiments[81] which suggest that the NH_4^- ion is best described as a solvated hydride ion. This parallels the behavior of $[ROHF]^-$ complex ions in that the structure of the solvated anion reflects the relative proton affinities of the proton-bound anions. Molecular hydrogen is a stronger acid than ammonia,[58] thus the complex resembles NH_3---H^- rather than H_2---NH_2^-. Photoelectron spectroscopic

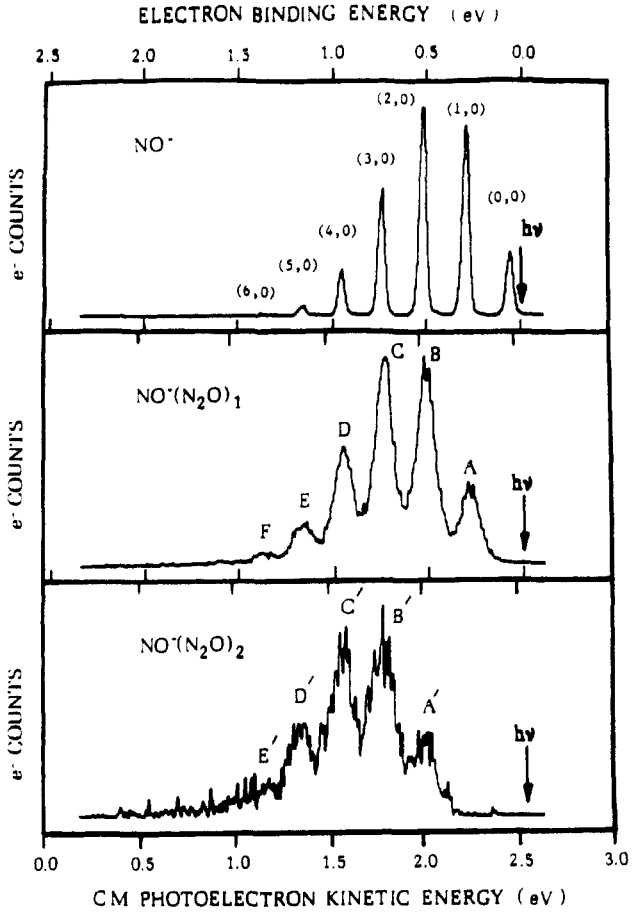

Figure 4. Photoelectron spectra of free and solvated nitric oxide ion (ref 82). Lower electron kinetic energy corresponds to higher energy transitions from the anion to the neutral. Reprinted with permission of the authors.

studies of larger hydride–ammonia complexes and ammonia-solvated amide ions are forthcoming.[79b]

Figure 4 displays the photoelectron (photodetachment) spectra of the gas-phase negative cluster ions $NO^-(N_2O)_1$ and $NO^-(N_2O)_2$ obtained by using 2.540-eV photons in a coaxial laser-ion beam photoelectron spectrometer.[82] Both spectra exhibit structured photoelectron spectral patterns which strongly resemble that of free NO^-, but which are shifted to successively lower electron kinetic energies with their individual peaks broadened. Each is interpreted in terms of a largely intact NO^- solvated by nitrous oxide molecule(s). For both $NO^-(N_2O)_1$ and $NO^-(N_2O)_2$, the ion–solvent dissociation energies for the loss of a single N_2O solvent molecule were approximated as 4.6 kcal/mol.[82] Electron affinities were also determined and found to increase with cluster size.

The aforementioned photodetachment experiments on solvated anions result in measurements that complement the data (i.e., H-bond energies) determined by using fluoride-exchange equilibria measurements[72,83] and HPMS clustering equilibria experiments.[84,85] All of the studies on solvated anions are important in that the elucidation of solvent interactions helps in understanding the transition from gas-phase ion behavior to solution-phase ion behavior.

In a somewhat analogous venture, work that aspires to bridge microscopic, molecular models of small (2–100 atoms) metal clusters to macroscopic bulk metal surfaces is in progress. Photodetachment of metal cluster negative ions[86] resulted in the experimental determination of EA as a function of cluster size. Experiments like these, in conjunction with predictions from ab initio calculations[87] modeling the electronic properties of metal clusters and their dependence on cluster size (up to 90 atoms), should ultimately provide a detailed view of the electronic structure of small metallic species. This information represents the microscopic limit of bulk surface properties, studied extensively by photoelectron spectroscopy (XPS, UPS).[88] To date, cluster negative ion beams of Ni, Nb, Cu, Ag, Si, Ge, GaAs, and Rb have been generated. For the Ni, Nb, and Cu clusters, photodetachment is the only decay channel observed. Estimates for the EAs of various Cu clusters indicated that the EA increases with n (n is the number of atoms in the cluster) and is higher for odd-n clusters. Similar results were found for GaAs clusters. In the Ag, Si, and Ge clusters, photofragmentation was found to compete with photodetachment. The photoelectron spectra of Rb_2^- and Rb_3^- are highly structured and exhibit transitions to several electronic states of the corresponding neutrals.

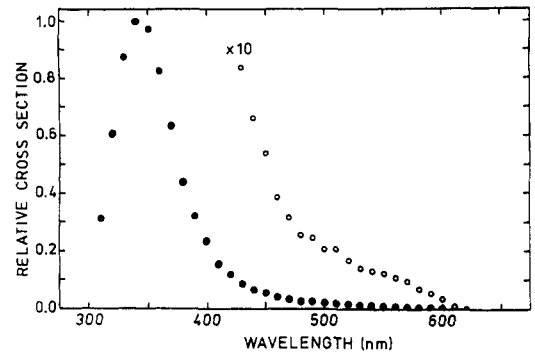

Figure 5. Photodetachment spectrum of phenylacetaldehyde enolate ion. Reprinted with permission from *J. Am. Chem. Soc.*, *99*, 7263. Copyright 1977 American Chemical Society.

V. Investigation of Electronic Transitions by Photodetachment Spectroscopy

A. Autodetaching Electronic Excited States in Anions

Electronically excited states of negative ions, like those in most neutrals, typically have energies of several electronvolts. Ionization potentials of neutrals are typically 10–15 eV, but the electron affinities (the corresponding energy to lose an electron from the negative ion) are generally less than 3 eV. Thus most excited electronic states in anions are unbound. Since a transition to an electronic excited state of the anion represents an alternative pathway for electron loss, these processes appear as resonances superimposed on the integral continuum photodetachment spectrum, provided that the probability for accessing the excited state is large enough to compete with direct photodetachment. Such autodetaching electronic excited states in anions have been observed in the photodetachment spectra of phenoxides,[89a,b] linear polyene anions,[89c] enolate anions[89d] (an example of which is shown in Figure 5), the cyclooctatetrenyl and perinaphthenyl anions,[89e] and, most recently, the benzyl and anilide anions.[57] These gas-phase experiments allow unambiguous assignment of excited-state transition energies, free from counterion and solvent effects. The resonances tend to be broad and featureless, indicative of

a short-lived state high in energy and strongly coupled to the neutral and free electron.

"Bound" electronic excited states observed in photodetachment spectra are those whose ground vibrational state is lower in energy than that of the neutral, yet which have some ro-vibrational levels higher in energy than the neutral. Some of these states can autodetach. In autodetachment, vibrational or rotational energy must be transferred into electronic degrees of freedom (Born–Oppenheimer breakdown). This coupling and the selection rules for the transition to the neutral and free electron (governed by energy, angular momentum, and parity conservation) often result in long-lived excited states of the anion. Transitions from the ground state of the anion to ro-vibrational levels of the bound electronic excited state that subsequently autodetach appear as (narrow) resonances superimposed on the rising background of direct photodetachment.

Few examples of bound valence excited states in molecular negative ions are known. One such system is the C_2^- anion, whose photodetachment spectrum has been measured to obtain both spectroscopic information[90a,b] and autodetachment rates.[90c] Another is the CH^- ion, which has a bound metastable electronic excited state. Both the energy[90d] and radiative lifetime[27] of this state have been measured.

The photodetachment spectrum of acetophenone enolate[91] contained narrow resonances, indicative of transitions to a bound, autodetaching state. These resonances appeared near threshold and could not be attributed to valence excited states.[92] Instead it was postulated that the bound excited state was a low-energy, diffuse state in which the electron was bound by an interaction with the permanent dipole moment of the neutral. The possibility of the existence of dipole-supported states had been proposed by theoreticians for many years. The states are analogous to Rydberg states, yet have a much smaller attractive potential since the electron is bound by a charge–dipole rather than coulombic potential. The problem of a charge bound by a dipole was first solved by Fermi and Teller.[93] A comprehensive review of other contributions to the problem is provided by Turner.[94] Especially pertinent to the study of dipole states in molecular anions is the inclusion of the rotation of the dipolar field by Garrett.[95]

Since dipole-supported excited states are bound by the molecular dipole moment, one expects stable molecular anions whose neutrals possess large dipole moments to exhibit these states. The following conditions must be satisfied in order that threshold resonances be observed: (1) the dipole-supported state must exist; (2) the transition probability to the excited state must be comparable to the transition probability for direct photodetachment; (3) the excited state must be sufficiently long-lived so that the resonance is measurably sharp against the background of direct photodetachment cross section; and (4) the autodetachment rate must be faster than radiative rates.[96] ICR photodetachment experiments are well suited for exploratory studies, since a wide variety of molecular anions can be generated and trapped and probed with reasonable resolution (1 cm^{-1}) over the entire visible and near IR wavelength regions.[2a] Many systems have now been observed to exhibit these states, including acetaldehyde enolate,[97] cyanomethyl anion,[98] acetyl fluoride enolate,[99] and the *p*-fluoro-, *m*-fluoro-, *p*-(*tert*-butyl)- and *m*-methyl-substituted acetophenone enolate anions.[92] As a test of the semiclassical model, the photodetachment spectra of the *o*- and *p*-benzoquinone radical anions (OBQ and PBQ, respectively) were recorded.[100] In this pair of ions the neutral dipolar core could be varied without substantially changing the electronic structure of the anions. Symmetrical PBQ has no dipole moment, while that in OBQ is estimated[101] to be approximately 5 D. Resonances at the threshold of electron photodetachment were present only for the OBQ anion, consistent with the picture that a large dipole moment is required for a quasi-bound-state to exist. The photodetachment spectra of some of these anions have been analyzed in detail.

Acetaldehyde enolate was studied initially by ICR and then coaxial ion-laser beam photodetachment spectroscopy.[97] The vibrational frequency of the torsional mode in the anionic ground state was obtained as 375 cm^{-1}, in good agreement with data from photoelectron studies.[102] Resolution of the vibrational bands into individual rotational transitions (made possible by the ultrahigh, 0.0007 cm^{-1}, resolution of the coaxial beam apparatus) allowed the determination of the rotational constants for the ground and excited states of the anion. These, in comparison to the rotational constants of the neutral radical, known from laser-induced fluorescence studies,[103] provide additional support for the dipole-state model. The rotational constants (and thus the geometry) of the dipole-supported state were remarkably similar to those of the radical, indicating that the electron in the excited state is in a diffuse orbital and does not significantly perturb the core. In addition to structural information, the study afforded information about the autodetachment dynamics and the binding energy of the dipole-supported state. The binding energy is the energy of the rotationless, vibrationless level of the excited state with respect to that of the neutral and free electron. Assignment of the binding energy was based on the absence of transitions to the lower rotational levels in the excited state. This is an estimate since the exact mechanism for autodetachment is not known. For acetaldehyde enolate the binding energy was estimated as 5 cm^{-1}. The spectrum contained surprisingly few bands; transitions to J levels (rotational quantum number N is equivalent to J in closed-shell anions) containing only 20 cm^{-1} of energy (over the binding energy) were too broad to be distinguished from background direct photodetachment. Measured line widths indicated that the lifetime of the dipole state decreases rapidly as the rotational energy of the state increases.

The 1-cm^{-1} resolution photodetachment spectrum of cyanomethyl (both the hydride and the deuteride, shown in Figure 6) anion, the conjugate base of acetonitrile, has been reported.[98] The vibration frequencies of the out-of-plane methylene umbrella mode, 430 ± 20 and 280 ± 20 cm^{-1}, for the hydride and deuteride, respectively, were obtained. Since individual J levels could not be resolved, complete geometry determination was not reported, but those rotational constants obtained from the spectral assignment indicated a change from pyramidal geometry in the anion to planar geom-

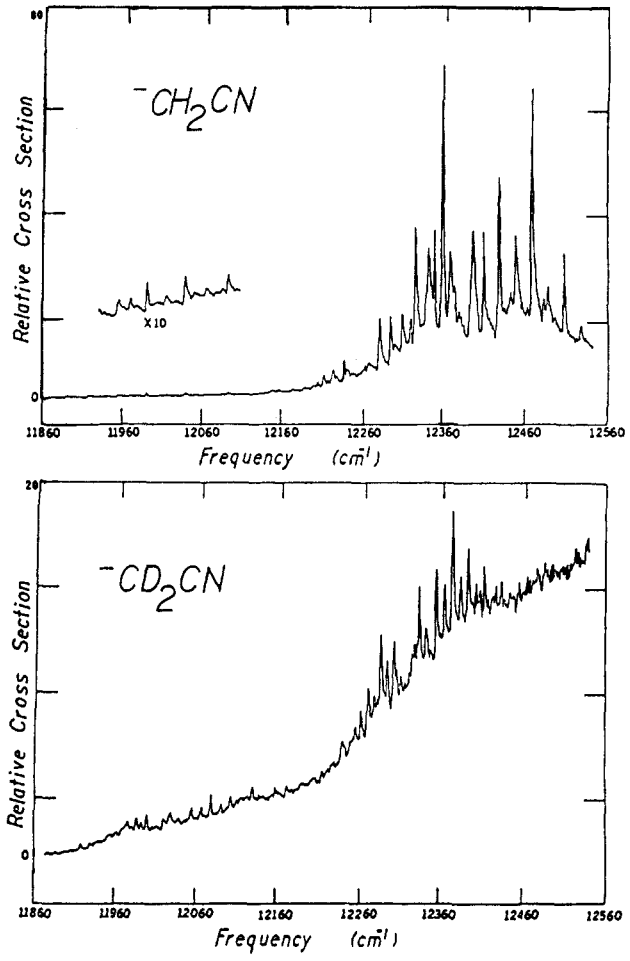

Figure 6. Photodetachment spectrum of cyanomethyl ($-h_2$) and ($-d_2$) anions. Reprinted with permission from *J. Chem. Phys.*, *84*, 5284. Copyright 1986 American Institute of Physics.

etry in the excited state. Further, the transition energies indicated stronger, shorter bonds in the excited state. The photodetachment spectra gave evidence of a binding energy much larger than that in acetaldehyde enolate, 160 ± 50 cm^{-1}. The adiabatic electron affinities, calculated from the sum of the rotationless transition energy and the binding energy of the dipole-supported state, were reported as 35.97 ($-h_2$) and 35.72 ($-d_2$) kcal/mol. These are a more accurate assignment than those reported from experiments conducted at resolution too low to resolve the resonances.[104] The observed transitions to rotational levels in the dipole-supported state are at energies below the threshold for direct photodetachment, verifying that rotational energy was transferred into electronic motion and utilized in electron detachment. Experiments measuring the ultrahigh-resolution photodetachment spectra of this anion will reveal information on the dynamics of the autodetachment in this system, likely to be very different from that seen in acetaldehyde enolate. Preliminary coaxial ion-laser beam photodetachment studies[105] on $^-CH_2CN$ indicate that excited-state lifetimes depend on J and not on K (that is, only the total angular momentum is important; the lifetimes begin drastically decreasing for high J, ~30 quanta, regardless of the total rotational energy of the molecule).

The photodetachment spectrum of acetyl fluoride enolate has also been analyzed in detail.[99] ICR photodetachment data afford information about the vibrational frequencies of the ground state of the anion. The methylene out-of-plane torsional mode, 494 cm^{-1}, was found to be higher than that of acetaldehyde, indicating a significant barrier to rotation. Assignment of the two O–C–F deformation modes, as 475 and 694 cm^{-1}, was accomplished. Complete analysis of the rotational transitions between the ground state and the dipole-supported excited state of the anion proved difficult in this system, due to the substantial geometry change between the two states. The absence of transitions to lower rotational levels of the excited state indicated a binding energy of approximately 35 cm^{-1}, again larger than that in acetaldehyde. Transitions to rotational states over 100 cm^{-1} above the binding energy were observed in the photodetachment spectrum. The measured line widths for transitions to upper rotational levels in general broadened with increasing rotational energy, but the effect of rotational energy on the lifetime of the excited state was not as dramatic as that in acetaldehyde.

The data obtained for these three systems can be compared to explain the nature of the dipole-supported state and the factors that influence the dynamics of autodetachment. In the absence of interference from direct photodetachment and under the assumption that the radiative rate is much slower than the autodetachment rate,[106] the resonance line widths give direct determination of the autodetachment rates and are therefore a measure of the lifetime of the autodetaching state. Two factors determine the lifetime of the state: coupling to the continuum and the attractive potential between the dipole and the exiting electron. In rotational autodetachment, transfer of angular momentum from molecular rotation to orbital angular momentum occurs. This process must conserve energy, angular momentum, and parity. In order to conserve energy and angular momentum, autodetachment from dipole states with a large binding energy requires a greater change in rotational angular momentum than does autodetachment from dipole states with a small binding energy. Rotational transitions with small ΔJ are favored. Coupling is best to low orbital angular momentum of the departing electron. Thus rotational-to-electronic coupling, manifested by the measured transition line width, should be different for states with different binding energies. In the three cases studied, acetaldehyde enolate's excited state is bound by only 5 cm^{-1}. Transitions to levels >20 cm^{-1} were not readily distinguishable from the background of direct photodetachment. In contrast, the photodetachment spectrum of cyanomethyl and acetyl fluoride contained transitions to rotational levels well over 100 cm^{-1} above the binding energy. In acetyl fluoride enolate, for a given amount of rotational energy, the lifetime of a level that autodetached with a $\Delta J = 4$ was approximately 4 times that of a state that autodetached with a $\Delta J = 0$. Because of the virtual match in the energy of the rotational levels between the excited state and the radical state, the coupling of orbital angular momentum of the anion into orbital angular momentum of the free electron may be more efficient in the acetaldehyde enolate system.

The dipole–electron attractive interaction in the excited state and molecular rotations affect the lifetime of the excited state. A semiclassical model predicts that the attraction (and hence binding energy) increases with

a larger dipole moment in the neutral core. The dipole moments are estimated to be 3.6, 4, and 5.7 D for acetaldehyde, cyanomethyl, and acetyl fluoride radicals, respectively. The binding energies do increase for those states with a larger dipole in the neutral core. The lifetimes of those states with the larger dipole are also less sensitive to the amount of rotational energy. On the basis of a semiclassical model and the results of Garrett,[95] one might predict that rotation of the dipole moments would not affect the lifetime of the dipole-supported state in cyanomethyl anion (since the dipole moment lies along the figure axis and rotation about this axis would not affect the orientation of the moment and the electron), yet would affect the lifetime of the dipole-supported state in acetaldehyde or in acetyl fluoride. The data, however, do not afford any definitive proof to validate this simple picture. Another factor which may influence the lifetime of the excited state is motion that rotates the orbital losing the electron, which can enhance rotational-to-electronic coupling, as was seen[107] in the case of vibrational autodetachment in NH^-.

In summary, studies of the photodetachment spectroscopy of molecular anions containing dipole-supported states have resulted in spectroscopic information for a number of molecular anions.[108] The nature of dipole-supported states and the dynamics of rotational autodetachment have also been more fully explained. In addition to those systems that have been mentioned and studied in great detail, the photodetachment spectra of many anions,[109] for instance, the enolates of cyclobutanone, 1,1,1-trifluoroacetone, methyl vinyl ketone, propionaldehyde, and methyl acetate, contain threshold resonances characteristic of transitions to dipole-supported states. Since these are large, polyatomic systems, assignment of the resonances to specific vibrational (rotational) transitions is difficult. Nonetheless, the large number of anions exhibiting dipole states provides validity to the assertion that such states are a general phenomenon.

B. Electronic Excited States in Neutrals

Photodetachment spectroscopy can be applied to the investigation of the electronic excited states in the neutrals. Detachment from the ground state of an anion to different final states (e.g., spin-orbit, triplet-singlet) in a neutral is evidenced by multiple onsets in the photodetachment spectra. The energy differences between the transitions directly yield the energy splitting. In optimum cases, cross-section modeling and ab initio calculations can be used to determine the relative ordering of these states. Since molecules containing unfilled valence levels are particularly reactive (i.e., carbenes, arenes, nitrenes) and experiments probing their spectroscopy are difficult, the use of photodetachment to probe neutrals by way of the anion is a viable alternative scheme.

Photodetachment has been used to study substituted nitrenes. The first direct measurement of the singlet-triplet splitting in a substituted nitrene was that for phenyl nitrene.[110] Photodetachment studies on other substituted nitrene anions has been attempted, but only with limited success.[111] Nitrene radical anions can in general be formed by low-energy electron impact on the corresponding parent azide. Methyl, ethyl, *tert*-butyl,

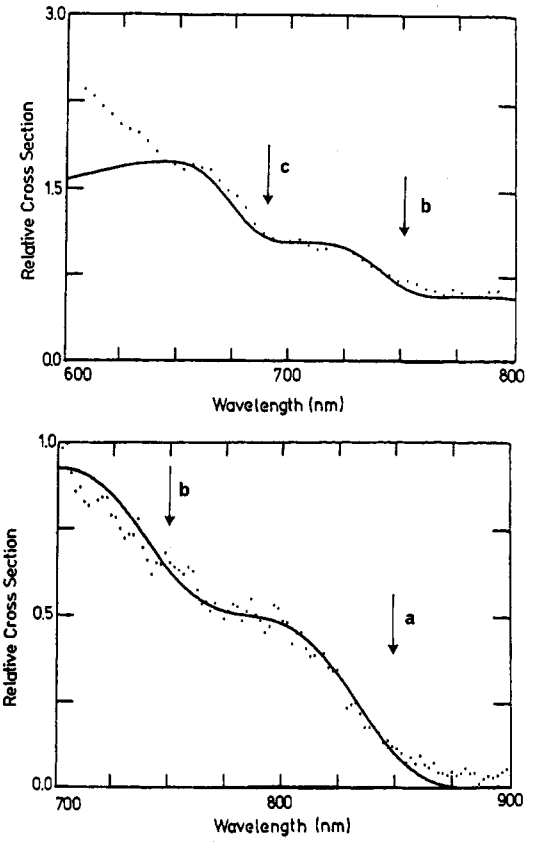

Figure 7. Photodetachment spectrum of phenylnitrene anion. The arrows indicate onsets for the transitions depicted in Figure 8. Reprinted with permission from *J. Am. Chem. Soc.*, *106*, 3443. Copyright 1984 American Chemical Society.

and *p*-toluenesulfonyl nitrene radical anions were formed in this way yet proved difficult to trap and photodetach because of the predominant reaction of the nitrene anion with the azide neutral forming azide anion. In the photodetachment spectrum of phenyl nitrene, shown in Figure 7, three onsets were observed. The results of ab initio calculations[112] (which predicted the electronic states of the neutral accessible from the ground state of the anion and provided a basis for the relative ordering of these states) and theoretical cross-section calculations, employing the one-electron formalism of Reed,[31] enabled these onsets to be assigned as transitions to the ground-state triplet and first and upper singlet states. These are shown in Figure 8. Fits to the theoretical cross-section behavior indicated that the observed onsets were direct photodetachment transitions, rather than transitions to excited vibrational levels of one of the electronic states. Since the data show sharp rather than broad and shallow onsets, the transitions were taken to be those to excited-state levels rather than vibrational hot bands. The theoretically expected cross-section shapes for each of the three possible transitions were too similar to enable relative ordering of the spin levels in the radical. The measured singlet-triplet splittings in the phenylnitrene system, displayed in Table II, are much smaller than those in imidogen[113] (~4 kcal/mol compared to ~30 kcal/mol). This has been attributed to possible lessened contributions from the exchange and Coulomb interactions, because the orbitals have reduced spatial overlap.

Another highly reactive neutral studied by photodetachment was *o*-benzyne. *o*-Benzyne anion, $C_6H_4^-$, was prepared in a flowing afterglow negative ion source;

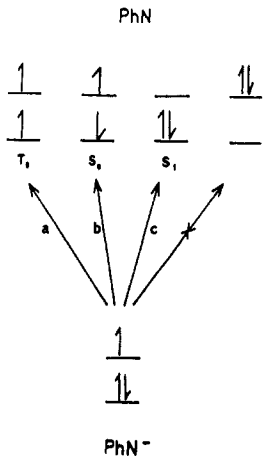

Figure 8. Low-energy transitions for the phenylnitrene anion photodetachment. The two-electron transition is not expected to be observed in the detachment experiment. Reprinted with permission from *J. Am. Chem. Soc., 106*, 3443. Copyright 1984 American Chemical Society.

TABLE II. Absolute and Relative Energies for Electronic Levels in Phenylnitrene[110]

state	absolute energy, kcal/mol	relative energy, kcal/mol
T_0	33.7 ± 0.3	0
S_0	38.0 ± 0.4	4.3 ± 0.4
S_1	42.5 ± 0.5	8.8 ± 0.5

transitions to the singlet ground state and (previously unobserved) lowest triplet state of the neutral were measured by photoelectron spectroscopy,[114] providing measurements of both the electron affinity, 12.9 + 0.2 kcal/mol, and singlet-triplet splitting, 37.7 + 0.6 kcal/mol, in the neutral.

VI. Vibration-Induced Electron Detachment

A. Experimental Evidence

Infrared multiple photon (IRMP) photoactivation typically results in fragmentation (dissociation process occurring on the electronic ground-state potential-energy surface). Since most bond dissociation energies (3–5 eV) in negative ions are larger than adiabatic electron affinities (often <3 eV), however, one might expect electron detachment to compete favorably with fragmentation, if it were the lower energy reaction pathway. Indeed, this premise was shown to be true.[115] IRMP activation under collisionless conditions in an ICR experiment resulted in electron detachment from the benzyl,[115,116] allyl, 2,4-hexadienyl, cycloheptadienyl, and anilide anions[116] and from hexafluorosulfide anion.[117] In these experiments the molecular anions sequentially absorbed 5–10 IR photons, supplied by a high-powered, pulsed CO_2 laser, in order to be activated to high enough internal energies to autodetach. These studies reported the wavelength dependence on photodetachment yield and a phenomenological cross section for the IRMP absorption (derived from photodetachment yield vs. fluence behavior, in conjunction with steady-state approximations[118]). IRMP-induced electron detachment is an interesting contrast to the autodetachment produced by optical excitation (as discussed in section V).

The aforementioned IRMP experiments do not provide any insight into the V-E mechanism that presumably drives the detachment process because of the lack of any measured detachment rates or even information on the relative efficiency of the detachment process. The nature of the IRMP activation and ICR spectrometry precludes any direct measurement of the rate constant for loss of an electron. Vibrational relaxation does not occur on the time scale of activation, since the duration of the IR pulse, ~3 μs, is much shorter than that of radiative (ms) or collisional (tens of ms at the pressures used in the ICR experiments) deactivation. Ions absorb photons at a rate determined by the laser intensity.[119] As the photons are absorbed, the vibrational energy is rapidly randomized to all other vibrational degrees of freedom in the molecule. Eventually subsequent absorptions excite the molecule to vibrational levels high enough in energy for autodetachment to occur. Autodetachment is observed when the detachment rate becomes competitive with the pumping rate. This is often above the thermodynamic threshold (the adiabatic electron affinity) for autodetachment. Both the photon pumping rate and probably even the slowest of autodetachment rates are fast on the ICR time scale (millisecond resolution). One problem inherent in the IRMP activation process is that it is impossible to determine precisely the total energy content of the anion, and in the ICR experiments it is not known at which vibrational energy level[120] autodetachment occurred.

The rate constant for electron detachment can in principle be indirectly determined from an experiment in which an IRMP-activated anion detached an electron in competition with a well-defined reaction. Branching experiments used to determine autodetachment rates indirectly are of general applicability, assuming a competing reaction with known mechanism and energetics (so that the reaction rate constant can be reasonably approximated) exists, preferably close in energy to the autodetachment threshold. Unimolecular dissociation reactions, frequently induced by IRMP activation, can serve as a competing pathway, since their reaction rates can be calculated by RRKM theory.[120] In such an experiment, acetone enolate ion was formed and IRMP activated in an ICR; branching between unimolecular fragmentation and vibration-induced electron detachment was observed.[121] Thermodynamic considerations enabled the thresholds for both channels to be estimated: 42 kcal/mol for autodetachment[2a] and 60–65 kcal/mol for fragmentation.[122] The (energy-dependent) rate constant for the fragmentation pathway was estimated[123] as approximately 10^6–10^7 s^{-1}, 3–6 kcal/mol above threshold. The observation of branching requires that the autodetachment rate constant be the same order of magnitude in this energy range (i.e., ~20 kcal/mol above the autodetachment threshold). Below the dissociation threshold, the autodetachment rate constant must be less than the pumping rate[119] or the anion would never be further activated to the dissociation threshold. This experiment thus indirectly determined the autodetachment rate constant as 10^7 s^{-1} at approximately 20 kcal/mol above threshold and $<10^7$ s^{-1} at threshold for autodetachment. Another branching experiment was that for IRMP-activated siloxide ions, trimethyl siloxide, and dimethyl siloxide ions, which were observed to undergo electron loss and unimolecular decomposition.[124] The trimethyl siloxide ion, sim-

ilar to *tert*-butoxide ion,[125] decomposed to give dimethylsilanone enolate (the silicon analogue of acetone enolate ion) and methane upon irradiation from a pulsed CO_2 laser. Unlike the case for *tert*-butoxide ion, however, electron-trapping experiments using CCl_4 (an efficient electron scavenger) indicated that vibration-induced electron detachment, the lower energy pathway, was also occurring. In fact, it was the dominant reaction. IRMP activation of dimethyl siloxide ion resulted in electron detachment and decomposition to dimethylsilanone enolate and molecular hydrogen. The decomposition was much more efficient in this system, compared to the trimethyl siloxide ion, observed even when very slow IR pumping rates ($10–10^2$ s^{-1} using a continuous wave CO_2 laser) were used. This indicated that the fragmentation and autodetachment channels are likely very close in energy. The observation of competing autodetachment and fragmentation, in conjunction with mechanistic considerations inferred by analogy to the *tert*-butoxide system,[125] was used to estimate an upper limit to the silicon oxygen π bond strength (62 kcal/mol). This study did not report any estimates of the autodetachment rates.

Vibration-induced electron detachment was utilized as an analytical method for isomer differentiation. In an experiment involving three $C_7H_7^-$ isomers,[126] the anions were irradiated in an ICR using a continuous wave CO_2 laser, and the recorded "action spectra" (photodecomposition, in this case, vibration-induced electron detachment, as a function of wavelength) served to identify three structurally distinct species. The spectra of cycloheptatrienyl and benzyl anions exhibited different wavelength dependences. The other isomer, norbornadienyl anion, did not undergo electron detachment.

B. Mechanism for Autodetachment Process

Simons has extended the original non Born–Oppenheimer coupled model, employed by Berry[127] to the vibrational autodetachment of Rydberg states in neutrals, to describe a physical mechanism for the coupling of nuclear motion into electronic degrees of freedom in the case of vibration-induced electron detachment from molecular anions.[128] The expression for the autodetachment rate[129]

$$W_{n\to n'} = 2\pi/\hbar |V_{Nk,n';A^-,n}|^2 \rho_e(\epsilon_n^- - \epsilon_{n'}^\circ) \qquad (10)$$

where ρ_e is the density of translational states of the detached electron, with kinetic energy equaling the energy difference between the vibrational energy levels of the anion and neutral (less the electron affinity), and $V_{Nk,n';A^-,n}$ is the coupling matrix element in which the subscripts Nk,n' and A^-,n label the $n'th$ (n^{th}) vibrational level in the neutral–electron continuum (anion) state. Nuclear motion affects the energy such that the electronic and vibrational wave functions mix; it is this coupling, embodied in the coupling matrix element, that gives rise to transitions between the anion and neutral molecule (plus free electron) states. Simons derived a set of propensity rules for vibration-induced autodetachment from this rate expression. These rules, which govern the electron detachment process only in the absence of the direct electronic mechanism,[44] state that transitions between vibrational states of the anion and neutral will occur efficiently if (1) the anion and neutral potential-energy surfaces approach or intersect one another in the region of "Q space" (Q corresponds to all of the vibrational and rotational degrees of freedom of the molecule) where the vibrational wave functions of the anion ($v = n$) and neutral ($v = n \pm 1$) are nonvanishing and the electronic force operator (that force which is exerted on the electron due to displacement along the Q coordinate) is large; (2) the shapes of the potential-energy curves of the anion and neutral are similar; and (3) low-energy electrons (in other words, a small Δv transition) are ejected. This development was intended as a tool for predicting and interpreting experimental results rather than an algorithm for calculating autodetachment rates. Simons outlined five "typical" anion and neutral potential-energy surface combinations (i.e., a case in which the neutral's molecular orbital, that orbital accepting the extra electron, is not bound for Q near the equilibrium geometry of the neutral but becomes bound as Q increases) and then made predictions as to the relative detachment rates with which specific anion/neutral pairs exemplifying these potential-energy curve classes should autodetach. Simons predicted that anilide should autodetach less efficiently than benzyl anion. Vibration-induced electron detachment was observed for both of these anions,[116] but because no rates were measured, the experimental results cannot validate the proposed propensity rules.

Simons and co-workers[130] conducted fully ab initio calculations, using the aforementioned autodetachment rate expression, on two "limiting case" examples, LiH^- and OH^-. These represent limiting cases in that, for LiH^-, the active orbital is strongly affected by the bond motion and the electron affinity[131] ($\sim$0.3 eV) is rather low and, for OH^-, the active orbital is nonbonding and not strongly affected by the motion of the O–H bond and the electron affinity[132] ($\sim$1.8 eV) is rather high. The results of the calculations found autodetachment lifetimes for various vibrational levels of LiH^- from $10^{-9}–10^{-10}$ s and, for OH^-, $10^{-5}–10^{-6}$ s. These calculated rates are in accord with the qualitative predictions. Autodetachment has been observed experimentally for OH^-, produced vibrationally hot in a beam by the two-step electron capture of H_2O^+ from Cs vapor.[133] In this experiment the average autodetachment lifetime could only be crudely approximated as exceeding 10^{-5} s. The NH^- ion, studied in a coaxial ion-laser beam experiment,[107] should be similar to the OH^- case because the active orbital is also π nonbonding. Since the electron affinity is rather low,[134] comparisons to the calculated rates for OH^- are not rigorous tests of the theory. The autodetachment lifetimes (lower bounds) for the $v = 1$ lower Λ-doublet levels of the anion, which decay to the $v = 0$ levels of the neutral, were 5 ns. This system showed a rotational enhancement effect (the upper Λ-doublet level's autodetachment lifetimes increased with rotational quanta) not predicted by the vibration-induced propensity rules.

Vibrationally excited anions prepared by heating or exothermic reactions rather than by IRMP (or single IR photon excitation) should also decay by the V-E coupling mechanism. Vibration-induced autodetachment is presumably involved in the nuclear excited Feshbach resonances observed in electron-scattering experiments,[135] in which the vibrationally excited anion

is a transient, bound species formed in the electron capture reaction

$$AB + e^- \rightarrow [AB^-]^* \rightarrow AB + e^- \quad (11)$$

Vibrationally excited anions are also formed by ion–molecule collisions of the type utilized in associative detachment experiments:[136]

$$A^- + B \rightarrow [AB^-]^* \rightarrow AB + e^- \quad (12)$$

Simple statistical models have been proposed[135] to predict the rates for autodetachment in processes of the type in eq 11. The statistical model does not require a physical mechanism for the V-E coupling.

In summary, photodetachment experiments supplement electron scattering or associative detachment experiments for studying the interesting and theoretically significant phenomena of vibrational-electronic coupling in autodetaching anions. These photodetachment experiments, however, are not without problems. The activation scheme employed must be such that the energy content of the vibrationally excited anion is precisely specified. This can be accomplished by pumping specific vibrational levels, fundamentals or overtones, with tunable IR or visible sources. The experiments must involve a method that either directly measures or indirectly ascertains the relative values of autodetachment rates for various anionic species. In order to test the available theoretical descriptions, diatomic systems have thus far been the most suitable anions to study, because the spectroscopy, electron affinities, and potential energy surfaces are either known or are more feasible to calculate and the active vibrational coordinate that induces autodetachment, Q, is uniquely specified.

Acknowledgments. We are grateful to the National Science Foundation for support of this work.

References

(1) Another process that can occur is photodissociation. This review concerns itself with experiments in which the process depicted by eq 1 dominates.
(2) (a) Drzaic, P. S.; Marks, J.; Brauman, J. I. In *Gas Phase Ion Chemistry*; Bowers, M. T., Ed.; Academic: Orlando, FL, 1984; Vol. 3. (b) Mead, R. D.; Stevens, A. E.; Lineberger, W. C. In *Gas Phase Ion Chemistry*; Bowers, M. T., Ed.; Academic: Orlando, FL, 1984; Vol. 3.
(3) Miller, T. M. *Adv. Electron. Electron Phys.* **1981**, *55*, 119.
(4) Berry, R. S.; Leach, S. *Adv. Electron. Electron Phys.* **1982**, *57*, 1.
(5) Another optical technique recently utilized for the first time to study the photodetachment process in molecular anions is laser optogalvanic spectroscopy: Klein, R.; McGinnis, R. P.; Leone, S. R. *Chem. Phys. Lett.* **1983**, *100*, 475.
(6) Janousek, B. K.; Brauman, J. I. In *Gas Phase Ion Chemistry*; Bowers, M. T., Ed.; Academic: New York, 1979; Vol. 2.
(7) (a) Grimsrud, E. P.; Caldwell, G.; Chowdhury, S.; Kebarle, P. *J. Am. Chem. Soc.* **1985**, *107*, 4627. (b) Chowdhury, S.; Grimsrud, E. P.; Heinis, T.; Kebarle, P. *J. Am. Chem. Soc.* **1986**, *108*, 3630. (c) Chowdhury, S.; Heinis, T.; Grimsrud, E. P.; Kebarle, P. *J. Phys. Chem.* **1986**, *90*, 2147.
(8) Lehman, T. A.; Bursey, M. M. *Ion Cyclotron Resonance Spectrometry*; Wiley-Interscience: New York, 1976.
(9) (a) Recently another type of ion trap, a Penning-type apparatus, was utilized to record the photodetachment spectrum of SeH^-: Stoneman, R. C.; Larson, D. J. *J. Phys. B* **1986**, *19*, L405.
(10) (a) McIver, R. T., Jr.; Hunter, R. L.; Ledford, E. B., Jr.; Locks, M. J.; Francl, T. J. *Int. J. Mass Spectrom. Ion Phys.* **1981**, *39*, 65. (b) Wronka, J.; Ridge, D. P. *Rev. Sci. Instrum.* **1982**, *53*, 491.
(11) The basic cyclotron equation and the magnet and CBD employed define the mass resolution; $\Delta m/m = 10^{-4}$ for mass 100 amu.
(12) McIver, R. T., Jr.; Ledford, E. B., Jr.; Hunter, R. L. *J. Chem. Phys.* **1980**, *72*, 2535.
(13) Marks, J.; Drzaic, P. S.; Foster, R. F.; Brauman, J. I.; Uppal, J. S.; Staley, R. H. *Rev. Sci. Instrum.*, in press.
(14) Anders, L. R.; Beauchamp, J. L.; Dunbar, R. C.; Baldeschwieler, J. D. *J. Chem. Phys.* **1978**, *45*, 111.
(15) Marshall, A. G. *Acc. Chem. Res.* **1985**, *18*, 316.
(16) (a) Branscomb, L. M. *Atomic and Molecular Processes*; Bates, D. R., Ed.; Academic: New York, 1962; p 112. (b) Smith, S. J. *Methods Exp. Phys.* **1972**, *7a*, 179.
(17) The expression assumes a monochromatic radiation source. For broad bandwidth experiments one needs to integrate over the spectral distribution function.
(18) Moylan, C. R.; Dodd, J. A.; Han, C. C.; Brauman, J. I. *J. Chem. Phys.*, in press.
(19) Steiner, B. *J. Chem. Phys.* **1968**, *49*, 5097.
(20) Su, T.; Bowers, M. T. *J. Chem. Phys.* **1973**, *58*, 3027. The number of collisions is given by $N_{coll} = k_{ADO}[M]t$, where [M] is the pressure of the neutral gas and t is the time the ion is trapped.
(21) Rosenfeld, R. N.; Jasinski, J. M.; Brauman, J. I. *J. Am. Chem. Soc.* **1979**, *101*, 3999.
(22) (a) Kim, M. S.; Dunbar, R. C. *Chem. Phys. Lett.* **1979**, *60*, 247. (b) Jasinski, J. M.; Brauman, J. I. *J. Chem. Phys.* **1980**, *73*, 6191. (c) Lev, N. B.; Dunbar, R. C. *J. Phys. Chem.* **1983**, *87*, 1924. (d) Barfknecht, A. T.; Brauman, J. I. *J. Chem. Phys.* **1986**, *84*, 3870.
(23) Collison efficiency = quenching rate constant/collision rate constant.
(24) For instance, the equilibrium constant measured for the charge-transfer reaction between *tert*-butoxide and sulfur dioxide (Fukuda, E. K.; McIver, R. T., Jr. *J. Chem. Phys.* **1982**, *77*, 4942) was undoubtedly affected by the internal energy of the alkoxide ion (formed by a ~27 kcal/mol exothermic reaction), since it led to an anomalously high electron affinity for SO_2. See: Caldwell, G.; Kebarle, P. *J. Chem. Phys.* **1984**, *80*, 577.
(25) CCl_4 is known to capture bound electrons efficiently (i.e., from Rydberg excited atoms); this process does not occur to an appreciable extent since the energetics are not feasible for the ions present in our experiment. The increase in the chloride ion signal is only detected following the laser shot.
(26) Okumura, M.; Yeh, L. I. C.; Normand, D.; Van den Biesen, J. J. H.; Bustamente, S. W.; Lee, Y. T. *Tetrahedron* **1985**, *41*, 1423.
(27) Okumura, M.; Yeh, L. I. C.; Normand, D.; Lee, Y. T. *J. Chem. Phys.* **1986**, *85*, 1971.
(28) Wigner, E. P. *Phys. Rev.* **1948**, *73*, 1002.
(29) (a) Burch, D. S.; Smith, S. J.; Branscomb, L. M.; Geltman, S. *Phys. Rev.* **1958**, *111*, 504. (b) O'Malley, T. F. *Phys. Rev.* **1965**, *137*, 1668.
(30) Geltman, S. *Phys. Rev.* **1958**, *112*, 176.
(31) Reed, K. J.; Zimmerman, A. H.; Andersen, H. C.; Brauman, J. I. *J. Chem. Phys.* **1976**, *64*, 1368.
(32) An example is HC_2^-: Janousek, B. K.; Brauman, J. I. *J. Chem. Phys.* **1979**, *71*, 2057.
(33) Non-Wigner threshold behavior was first treated by O'Malley (ref 29b) for the case of polarizable atomic anions.
(34) Engelking, P. C. *Phys. Rev. A* **1982**, *26*, 740.
(35) Schultz, P. A.; Mead, R. D.; Jones, P. L.; Lineberger, W. C. *J. Chem. Phys.* **1982**, *77*, 1153.
(36) Engelking, P. C.; Herrick, D. R. *Phys. Rev. A* **1984**, *29*, 2425.
(37) Conventional Slater orbital exponents do not adequately describe the anion orbitals; exponents were chosen semiempirically.
(38) Stehman, R. M.; Woo, S. B. *Phys. Rev. A* **1979**, *20*, 281.
(39) Stehman, R. M.; Woo, S. B. *Phys. Rev. A* **1981**, *23*, 2866.
(40) Clodius, W. B.; Stehman, R. M.; Woo, S. B. *Phys. Rev. A* **1983**, *28*, 1160.
(41) Clodius, W. B.; Stehman, R. M.; Woo, S. B. *Phys. Rev. A* **1983**, *27*, 333.
(42) Rau, A. R. P.; Fano, U. *Phys. Rev. A* **1971**, *4*, 1751.
(43) Hotop, H.; Patterson, T. A.; Lineberger, W. C. *Phys. Rev. A* **1973**, *8*, 762.
(44) The intensities of photodetachment, like other electronic transitions, are governed by the Franck–Condon principle.
(45) Moylan, C. R.; Brauman, J. I. *Annu. Rev. Phys. Chem.* **1986**, *34*, 187.
(46) The ionization potential of hydrogen is 313.6 kcal/mol: Stull, D. R., Prophet, H., Eds. JANAF *Thermochemical Tables*; National Standard Reference Data Series, U.S. National Bureau of Standards NSRDS-NBS 37; U.S. Government Printing Office: Washington, DC, 1971.
(47) Golden, D. M.; McMillen, D. F. *Annu. Rev. Phys. Chem.* **1982**, *33*, 493.
(48) (a) Moylan, C. R.; Brauman, J. I. *J. Phys. Chem.* **1984**, *88*, 3175. (b) Moylan, C. R.; Jasinski, J.; Brauman, J. I. *Chem. Phys. Lett.* **1983**, *98*, 1.
(49) HPMS experiments confirm this assertion: Meot-Ner, M.; Sieck, L. W. *J. Phys. Chem.* **1986**, *90*, 6687.

(50) Gray, P.; Waddington, T. C. *Proc. R Soc. London, A* **1956**, *235*, 481.
(51) Franklin, J. L.; Dibeler, V. H.; Reese, R. M.; Krauss, M. *J. Am. Chem. Soc.* **1958**, *80*, 298.
(52) Jackson, R. L.; Pellerite, M. J.; Brauman, J. I. *J. Am. Chem. Soc.* **1981**, *103*, 1802.
(53) Illenberger, E.; Comita, P. B.; Brauman, J. I.; Fenzlaff, H. P.; Henri, M.; Heinrich, N.; Koch, W.; Frenking, G. *Ber. Bunsen-Ges Phys. Chem.* **1985**, *89*, 1026.
(54) Pellerite, M. J.; Jackson, R. L.; Brauman, J. I. *J. Phys. Chem.* **1981**, *85*, 1624.
(55) Brauman, J. I. *Frontiers of Free Radical Chemistry*; Pryor, W. A., Ed.; Academic: New York, 1980; p 23.
(56) Okabe, H. *Photochemistry of Small Molecules*; Wiley-Interscience: New York, 1978; p 261.
(57) Drzaic, P. S.; Brauman, J. I. *J. Phys. Chem.* **1984**, *88*, 5285.
(58) Bartmess, J. E.; McIver, R. T., Jr. In *Gas Phase Ion Chemistry*; Bowers, M. T., Ed.; Academic: Orlando, FL, 1979; Vol. 3.
(59) McDonald, R. N.; Chowdhury, A. K.; Setser, D. W. *J. Am. Chem. Soc.* **1981**, *103*, 6599.
(60) (a) Salomon, K. A. Ph.D. Thesis, Stanford University, Stanford, CA. (b) Salomon, K. A.; Wetzel, D.M.; Berger, S.; Brauman, J. I., manuscript in preparation.
(61) Janousek, B. K.; Zimmerman, A. H.; Reed, K. J.; Brauman, J. I. *J. Am. Chem. Soc.* **1978**, *100*, 6142.
(62) Janousek, B. K.; Reed, K. J.; Brauman, J. I. *J. Am. Chem. Soc.* **1980**, *102*, 3125.
(63) Nimlos, M. R.; Ellison, G. B. *J. Am. Chem. Soc.* **1986**, *108*, 6522.
(64) Interaction of the filled π orbitals of the methyl group with the empty π antibonding orbitals of the Si atom results in net donation of electron density. Michl, J. *Tetrahedron* **1984**, *40*, 3845.
(65) Salomon, K. A.; Brauman, J. I., manuscript in preparation.
(66) Miller, T. A.; Stevens, A. E.; Lineberger, W. C. *Phys. Rev. A* **1986**, *33*, 3558.
(67) Golub, S.; Steiner, B. *J. Chem. Phys.* **1968**, *49*, 519.
(68) Moylan, C. R.; Dodd, J. A.; Brauman, J. I. *Chem. Phys. Lett.* **1985**, *118*, 38.
(69) Faigle, J. F. G.; Isolani, P. C.; Riveros, J. M. *J. Am. Chem. Soc.* **1976**, *98*, 2049.
(70) Detachment of precursor ion F^- sets in at 3.399 eV (Mead, R. D.; Stevens, A. E.; Lineberger, W. C. In *Gas Phase Ion Chemistry*; Bowers, M. T., Ed.; Academic: Orlando, FL, 1984; Vol. 3) and would obscure the photodetachment onset of the complex anion.
(71) Estimated as 8 ± 2 kcal/mol from: (a) Dill, J. D.; Allen, L. C.; Topp, W. C.; Pople, J. A. *J. Am. Chem. Soc.* **1975**, *97*, 7220. (b) Thomas, R. K. *Proc. R. Soc. London, A* **1975**, *A344*, 579. (c) Hinchliffe, A. *Adv. Mol. Relax. Interact. Processes* **1981**, *20*, 71.
(72) Larson, J. W.; McMahon, T. B. *J. Am. Chem. Soc.* **1983**, *105*, 2944.
(73) Caldwell, G.; Rozeboom, M. D.; Kiplinger, J. P.; Bartmess, J. E. *J. Am. Chem. Soc.* **1984**, *106*, 4660. This is a preliminary value reported from HPMS experiments and is currently being reinvestigated. Kebarle, P., personal communication.
(74) Drzaic, P. S.; Brauman, J. I. *J. Am. Chem. Soc.* **1982**, *104*, 13.
(75) Lifshitz, C.; Tiernan, T. O.; Hughes, B. M. *J. Chem. Phys.* **1973**, *59*, 3182.
(76) Edelson, D.; Griffiths, J. E.; McAfee, K. B., Jr. *J. Chem. Phys.* **1962**, *37*, 917.
(77) Hay, J. P. *J. Chem. Phys.* **1982**, *76*, 502.
(78) Grimsrud, E. P.; Chowdhury, S.; Kebarle, P. *J. Chem. Phys.* **1985**, *83*, 1059.
(79) (a) Coe, J. V.; Snodgrass, J. T.; Freidhoff, C. B.; McHugh, K. M.; Bowen, K. H. *J. Chem. Phys.* **1985**, *83*, 3169. (b) Snodgrass, J. T.; Coe, J. V.; Freidhoff, C. B.; McHugh, K. M.; Bowen, K. H. *J. Chem. Phys.*, submitted.
(80) (a) Kalcher, J.; Rosmus, P.; Quack, M. *Can. J. Phys.* **1984**, *62*, 1323. (b) Squires, R. R. In *Ionic Processes in the Gas Phase*; Amoster Ferreira, M. A., Ed.; NATO Advanced Science Institutes Series, Series C; Reidel: Dordrecht, The Netherlands, 1984; Vol. 118.
(81) Kleingeld, J. C.; Ingemann, S.; Jolonen, J. E.; Nibbering, N. M. M. *J. Am. Chem. Soc.* **1983**, *105*, 2474.
(82) Coe, C. V.; Snodgrass, C. T.; Freidhoff, C. B.; McHugh, K. M.; Bowen, K. H. *J. Chem. Phys.*, submitted.
(83) Larson, J. W.; McMahon, T. B. *J. Am. Chem. Soc.* **1982**, *104*, 5848.
(84) (a) Kebarle, P. *Annu. Rev. Phys. Chem.* **1977**, *28*, 445. (b) Kebarle, P.; Davidson, W. R.; French, M.; Cumming, J. B.; McMahon, T. B. *Faraday Discuss. Chem. Soc.* **1978**, *64*, 220.
(85) Keesee, R. G.; Lee, N.; Castleman, A. W., Jr. *J. Chem. Phys.* **1980**, *73*, 2195.
(86) (a) Zheng, L. S.; Brucat, P. J.; Pettiette, C. L.; Yang, S.; Smalley, R. E. *J. Chem. Phys.* **1985**, *83*, 4273. (b) Zheng, L. S.; Karner, C. M.; Brucat, P. J.; Yang, S. H.; Pettiette, C. L.; Craycraft, M. J.; Smalley, R. E. *J. Chem. Phys.* **1986**, *85*, 1681. (c) Lui, Y.; Zhang, Q. L.; Tittle, F. K.; Curl, R. F.; Smalley, R. E. *J. Chem. Phys.*, in press. (d) Leopold, D. G.; Hoe, J.; Lineberger, W. C. *J. Chem. Phys.*, in press. (e) McHugh, K. M.; Eaton, J. G.; Lee, G. H.; Snodgrass, J. S.; Bowen, K. H. *J. Chem. Phys.*, submitted.
(87) (a) Demuynck, J.; Rohmer, M. M.; Strich, A.; Veillard, A. *J. Chem. Phys.* **1981**, *75*, 3443. (b) Baetzold, R. C.; Mack, R. E. *J. Chem. Phys.* **1975**, *62*, 1513. (c) Melius, C. F.; Upton, T. H.; Goddard, W. A., III. *Solid State Commun.* **1978**, *28*, 501.
(88) Chaudhari, S. N.; Cheng, K. L. *Appl. Spectrosc. Rev.* **1980**, *16*, 187.
(89) (a) Richardson, J. H.; Stephenson, L. M.; Brauman, J. I. *J. Chem. Phys.* **1975**, *62*, 1580. (b) Richardson, J. H.; Stephenson, L. M.; Brauman, J. I. *J. Am. Chem. Soc.* **1975**, *97*, 2967. (c) Zimmerman, A. H.; Reed, K. J.; Brauman, J. I. *J. Am. Chem. Soc.* **1978**, *100*, 5595. (d) Zimmerman, A. H.; Reed, K. J.; Brauman, J. I. *J. Am. Chem. Soc.* **1977**, *99*, 7203. (e) Gygax, R.; McPeters, H. L.; Brauman, J. I. *J. Am. Chem. Soc.* **1979**, *101*, 2567.
(90) (a) Jones, P. C.; Mead, R. D.; Kohler, B. E.; Rosner, S. D.; Lineberger, W. C. *J. Chem. Phys.* **1980**, *73*, 4419. (b) Mead, R. D.; Heftner, U.; Schulz, P. A.; Lineberger, W. C. *J. Chem. Phys.* **1985**, *82*, 1723. (c) Heftner, U.; Mead, R. D.; Schulz, P. A.; Lineberger, W. C. *Phys. Rev. A* **1983**, *28*, 1429. (d) Kasdan, A.; Herbst, E.; Lineberger, W. C. *Chem. Phys. Lett.* **1975**, *31*, 78.
(91) Zimmerman, A. H.; Brauman, J. I. *J. Chem. Phys.* **1977**, *66*, 5823.
(92) Based on energetics arguments and substitution studies. Electron-donating and -withdrawing substituents to the phenyl ring shift valence transitions due to inductive effects on the energy of the HOMO, yet the narrow resonances followed the photodetachment threshold in all cases: Jackson, R. L.; Zimmerman, A. H.; Brauman, J. I. *J. Chem. Phys.* **1979**, *71*, 2088.
(93) Fermi, E.; Teller, E. *Phys. Rev.* **1947**, *72*, 406.
(94) Turner, J. E. *Am. J. Phys.* **1977**, *45*, 758.
(95) Garrett, W. R. *Phys. Lett.* **1970**, *5*, 393. *Phys. Rev. A* **1971**, *3*, 961. *J. Chem. Phys.* **1980**, *73*, 5721. *J. Chem. Phys.* **1982**, *77*, 3666.
(96) 10^{-6}–10^{-9} s, from studies involving open-shell cations: Maier, J. P.; Thommen, F. In *Gas Phase Ion Chemistry*; Bowers, M. T., Ed.; Academic: Orlando, FL, 1984; Vol. 3.
(97) (a) Jackson, R. L.; Hiberty, P. C.; Brauman, J. I. *J. Chem. Phys.* **1981**, *74*, 3705. (b) Lykke, K. R.; Mead, R. D.; Lineberger, W. C. *Phys. Rev. Lett.* **1984**, *52*, 2221. (c) Mead, R. D.; Lykke, K. R.; Lineberger, W. C.; Marks, J.; Brauman, J. I. *J. Chem. Phys.* **1984**, *81*, 4883.
(98) Marks, J.; Wetzel, D. M.; Comita, P. B.; Brauman, J. I. *J. Chem. Phys.* **1986**, *84*, 5284.
(99) Marks, J.; Brauman, J. I.; Mead, R. D.; Lykke, K. R.; Lineberger, W. C., manuscript in preparation.
(100) Marks, J.; Comita, P. B.; Brauman, J. I. *J. Am. Chem. Soc.* **1985**, *107*, 3718.
(101) Nagakura, S.; Kuboyama, A. *J. Am. Chem. Soc.* **1954**, *76*, 1003.
(102) Ellison, G. B.; Engelking, P. C.; Lineberger, W. C. *J. Phys. Chem.* **1982**, *86*, 4873.
(103) Dimauro, L. F.; Heaven, M.; Miller, T. A. *J. Chem. Phys.* **1984**, *81*, 2339.
(104) Zimmerman, A. H.; Brauman, J. I. *J. Am. Chem. Soc.* **1977**, *99*, 3565.
(105) Lykke, K. R.; Neumark, D. M.; Andersen, T.; Trappa, V. J.; Lineberger, W. C. In *Laser Spectroscopy VII*; Hansch, T. W., Shen, Y. R., Eds.; Springer: Berlin, 1985; pp 130–133.
(106) Fano, U. *Phys. Rev.* **1961**, *124*, 1866.
(107) Neumark, D. M.; Lykke, K. R.; Andersen, T.; Lineberger, W. C. *J. Chem. Phys.* **1985**, *83*, 4364.
(108) Few experimental techniques are available for the study of negative ion spectroscopy. OH^- and OD^- have been studied by high-resolution photodetachment experiments: (a) Smith, S. J.; Branscomb, L. M. *Phys. Rev.* **1955**, *99*, 1657. (b) Branscomb, L. M. *Phys. Rev.* **1966**, *148*, 11. (c) Hotop, H.; Patterson, T. A.; Lineberger, W. C. *J. Chem. Phys.* **1974**, *60*, 1806. (d) Breyer, F.; Frey, P.; Hotop, H. *Z. Phys. A* **1981**, *300*, 7. (e) Schulz, P. A.; Mead, R. D.; Jones, P. L.; Lineberger, W. C. *J. Chem. Phys.* **1982**, *77*, 1153. OH^- and OD^- have also been studied by using velocity modulation spectroscopy: (f) Owrutsky, J. C.; Rosenbaum, N. H.; Tack, L. M.; Saykally, R. J. *J. Chem. Phys.* **1985**, *83*, 5338. (g) Rosenbaum, N. H.; Owrutsky, J. C.; Tack, L. M.; Saykally, R. J. *J. Chem. Phys.* **1986**, *84*, 5308. NH_2^- has been studied by using velocity modulation spectroscopy: (h) Tack, L. M.; Rosenbaum, N. H.; Owrutsky, J. C.; Saykally, R. J. *J. Chem. Phys.* **1986**, *85*, 4222. Vibration-induced autodetachment (see section VI) has been applied to obtain spectroscopic information on NH^- (ref 107).
(109) Marks, J. Ph.D. Thesis, Stanford University, Stanford, CA.
(110) Drzaic, P. S.; Brauman, J. I. *J. Am. Chem. Soc.* **1984**, *106*, 3443.

(111) Rynard, C. Ph.D. Thesis, Stanford University, Stanford, CA.
(112) Van-Catledge, F. A. (Du Pont), personal communication.
(113) Okabe, H. *Photochemistry of Small Molecules*; Wiley-Interscience: New York, 1970; p 193.
(114) Leopold, D. G.; Miller, A. E.; Lineberger, W. C. *J. Am. Chem. Soc.* **1986**, *108*, 1379.
(115) Rosenfeld, R. N.; Jasinski, J. M.; Brauman, J. I. *J. Chem. Phys.* **1979**, *71*, 1030.
(116) Meyer, F. K.; Jasinski, J. M.; Rosenfeld, R. N.; Brauman, J. I. *J. Am. Chem. Soc.* **1982**, *104*, 663.
(117) Drzaic, P. S.; Brauman, J. I. *Chem. Phys. Lett.* **1981**, *83*, 508.
(118) (a) Quack, M. *J. Chem. Phys.* **1979**, *70*, 1069. (b) Quack, M. *Ber. Bunsen-Ges. Phys. Chem.* **1979**, *83*, 1287. (c) Quack, M.; Humbert, P.; van den Bergh, H. *J. Chem. Phys.* **1980**, *73*, 247.
(119) The rate of photon absorption for high-powered pulsed IR lasers is about 10^7 s^{-1}. Use of low-power IR lasers, where pumping rates are ~ 10–10^3 s^{-1}, to activate anions presents too many complications (deactivation by radiative or collisional processes becomes competitive) to be a reliable source of rate information.
(120) Intramolecular energy randomization is much faster than sequential photon absorption and most reaction rates. Thus IRMP-activated processes can be described by statistical reaction rate (i.e., RRKM) theory. For polyatomics, internal energy randomization becomes increasingly rapid at high energies, due to the increase in density of states and anharmonic coupling. At high energy it is therefore more appropriate to discuss the energy levels of a molecule rather than specific quantum states.
(121) Foster, R. F.; Tumas, W.; Brauman, J. I. *J. Chem. Phys.* **1979**, *79*, 4644.
(122) Benson, S. W. *Thermochemical Kinetics*, 2nd ed.; Wiley-Interscience: New York, 1976.
(123) On the basis of calculations using the program of W. L. Hase and D. L. Bunker, Quantum Chemistry Program Exchange, No. 234, Indiana University.
(124) Tumas, W.; Salomon, K. E.; Brauman, J. I. *J. Am. Chem. Soc.* **1986**, *108*, 2541.
(125) Tumas, W.; Foster, R. F.; Brauman, J. I. *J. Am. Chem. Soc.* **1984**, *106*, 4053.
(126) Wight, C. A.; Beauchamp, J. L. *J. Am. Chem. Soc.* **1981**, *103*, 6499.
(127) Berry, R. S. *J. Chem. Phys.* **1966**, *45*, 1228.
(128) Simons, J. *J. Am. Chem. Soc.* **1981**, *103*, 3971.
(129) This is the "Fermi Golden rule" result of first-order time-dependent perturbation theory.
(130) Acharya, P. K.; Kendall, R. A.; Simons, J. *J. Am. Chem. Soc.* **1984**, *106*, 3402.
(131) Hotop, H.; Patterson, T. A.; Lineberger, W. C. *J. Chem. Phys.* **1974**, *60*, 1809.
(132) Liu, B.; O-Ohata, K.; Kirby-Docken, K. J. *Chem. Phys.* **1977**, *67*, 1850.
(133) Bae, Y. K.; Cosby, P. C.; Peterson, J. R. *Chem. Phys. Lett.* **1986**, *126*, 266.
(134) Engelking, P. C.; Lineberger, W. C. *J. Chem. Phys.* **1976**, *65*, 4323.
(135) Christophorou, L. G. *Adv. Electron. Electron Phys.* **1978**, *46*, 55.
(136) (a) Herzenberg, A. *Phys. Rev.* **1967**, *160*, 80. (b) Chen, J. C. Y. *Phys. Rev.* **1967**, *156*, 12.
(137) (a) Nimlos, M. R.; Ellison, G. B. *J. Phys. Chem.* **1986**, *90*, 2574. (b) Al-Za'al, M.; Miller, H. C.; Farley, J. W. *Chem. Phys. Lett.* **1986**, *131*, 56. (c) Coe, C. V.; Snodgrass, J. T.; Freidhoff, C. B.; McHugh, K. M.; Bowen, K. H. *J. Chem. Phys.* **1986**, *84*, 618. (d) Leopold, D. G.; Lineberger, W. C. *J. Chem. Phys.* **1986**, *85*, 51.